

Citation for published version:

An, Y, Ma, C, Zhang, N, Guo, Y, Degano, M, Li, Q & Zhou, S 2021, 'Calculation Model of Armature Reaction Magnetic Field of Interior Permanent Magnet Synchronous Motor with Segmented Skewed Poles', *IEEE Transactions on Energy Conversion*. <https://doi.org/10.1109/TEC.2021.3123359>

DOI:

[10.1109/TEC.2021.3123359](https://doi.org/10.1109/TEC.2021.3123359)

Publication date:

2021

Document Version

Peer reviewed version

[Link to publication](#)

© 2021 IEEE. Personal use of this material is permitted. Permission from IEEE must be obtained for all other users, including reprinting/ republishing this material for advertising or promotional purposes, creating new collective works for resale or redistribution to servers or lists, or reuse of any copyrighted components of this work in other works.

University of Bath

Alternative formats

If you require this document in an alternative format, please contact:
openaccess@bath.ac.uk

General rights

Copyright and moral rights for the publications made accessible in the public portal are retained by the authors and/or other copyright owners and it is a condition of accessing publications that users recognise and abide by the legal requirements associated with these rights.

Take down policy

If you believe that this document breaches copyright please contact us providing details, and we will remove access to the work immediately and investigate your claim.

Calculation Model of Armature Reaction Magnetic Field of Interior Permanent Magnet Synchronous Motor with Segmented Skewed Poles

Yuansheng An, Conggan Ma, *Senior Member IEEE*, Nic Zhang, Yue Guo, *Senior Member, IEEE*, Michele Degano, *Member IEEE*, Chris Gerada, *Senior Member IEEE*, Feifei Bu, *Senior Member IEEE*, Xiangrui Yin, Qiongyao Li, and Shengsen Zhou

Abstract—In an interior permanent magnet synchronous motor (IPMSM) with segmented skewed poles, the armature reaction magnetic field (AR-MF) changes nonlinearly due to the saturation of the rotor magnetic barrier. Meanwhile, this varies under different excitation currents. As a result, it is difficult to be calculated by means of analytical methods. In this paper, the calculation model of AR-MF of IPMSM is first established by vector superposition method, without considering the saturation effect of rotor and the slotting effect of stator. In the second step, the virtual magnetic field of the rotor is introduced to quantitatively calculate the influence of local inhomogeneous saturation on the AR-MF. The latter is derived by combining both the subdomain method and equivalent magnetic circuit method. The complex relative permeance is also introduced to establish the AR-MF accounting for the stator slotting effect. To validate the AR-MF calculation method proposed, an 8-pole 48-slot IPMSM with segmented skewed poles is considered as a case study, showing a comparison by both with finite element (FE) results and the electromagnetic torque measured on a test bench. The model proposed in this paper shows high accuracy and fast computation with respect to FE analysis.

Index Terms—Interior permanent magnet synchronous motor, segmented skewed poles, armature reaction magnetic field, virtual magnetic field of rotor magnetic barrier, local inhomogeneous saturation.

I. INTRODUCTION

IPMSM with segmented skewed poles has been subject of research and gained more interest for its high power density, high torque density and wide speed range [1]–[5]. The armature reaction magnetic field (AR-MF) affects the torque, efficiency,

vibration and noise performance of the motor [2]. The magnetic field of the IPMSM is difficult to calculate due to its nonlinear behavior is due to the saturation of rotor magnetic barrier [1]. Therefore, the calculation of AR-MF is an important and difficult problem.

The calculation methods used to compute AR-MF are either analytical or using finite element (FE) analysis. The latter can take the influence of saturation on the AR-MF into consideration, and its accuracy is high [3][6]. However, it is time-consuming, which is not desired when a fast performance evaluation of a motor is required in the industry. The analytical methods presented in literature are based on the following: magnetic potential-permeance [2][7]–[13], vector superposition [14][15], subdomain models [4][16]–[19], winding functions [1][5][20] and magnetic equivalent circuit [21]–[23]. The magnetic potential-permeance method is widely used, in which the slotting effect can be calculated by the permeance function [7]–[13]. However, this method usually assumes that the permeability of the core is infinite, so the nonlinear variation of magnetic field caused by core saturation cannot be considered. In [2], the complex relative permeance of rotor magnetic barrier is introduced, and the influence of rotor magnetic barrier saturation on AR-MF can be calculated. However, the complex relative permeance of rotor magnetic barrier still needs to be calculated by finite element simulation, which reduces the calculation efficiency. Alternatively, the spatial distribution of the AR-MF can be obtained by vector superposition method, while the saturation effect is ignored due to the neglect of rotor structure [14][15]. On the other hand, subdomain method uses boundary conditions to solve the AR-MF, and the accuracy will

Manuscript received Month xx, 2021; revised Month xx, 2021; accepted Month x, xxxx. This work was supported in part by National Natural Science Foundation of China under Grant 51975141 and Grant 51605112, in part by Natural Science Foundation of Shandong Province under Grant ZR2015EQ020, and in part by the 2018 Open Fund of State Key Laboratory of Comprehensive Technology on Automobile Vibration and Noise & Safety Control under Grant 2018-03. (Corresponding author: Conggan Ma, 86-178-6272-2800; e-mail: maconggan@163.com)

Yuansheng An, Conggan Ma, Qiongyao Li, and Shengsen Zhou are with Harbin Institute of Technology-Weihai, Weihai, 264209, China (e-mail: anyuansheng@126.com; maconggan@163.com; 18369186012@163.com; zhoushengsen@126.com).

Nic Zhang is with University of Bath, Bath, the UK (email: qz254@bath.ac.uk).

Yue Guo is with Coventry University, Coventry, the UK (e-mail: yue.guo@coventry.ac.uk).

Michele Degano and Chris Gerada are with University of Nottingham, Nottingham, the UK (e-mail: michele.degano@nottingham.ac.uk; chris.gerada@nottingham.ac.uk).

Feifei Bu is with Nanjing University of Aeronautics and Astronautics, Nanjing, China (e-mail: bufeifei1984@163.com).

Xiangrui Yin is with State Key Laboratory of Comprehensive Technology on Automobile Vibration and Noise & Safety Control, China First Automobile Works Group, Changchun, China (e-mail: yinxiangrui@faw.com.cn).

> REPLACE THIS LINE WITH YOUR PAPER IDENTIFICATION NUMBER (DOUBLE-CLICK HERE TO EDIT) <

be high if there is no core saturation [4][16]-[19]. However, the boundary conditions increase significantly the complexity of the magnetic field calculation if the saturation is considered. In addition, the AR-MF can also be obtained from the winding function theory [20]. However, the saturation effect cannot be calculated simply by this method. In [5], the saturation effect is calculated by a combination of winding function and magnetic equivalent circuit methods. The latter assumes that the flux lines are perpendicular to the interface between the core and the air gap. Therefore, it can only calculate the radial component of the magnetic field, but not the tangential. In order to make the calculation more accurate, either the finite element method needs to be combined [21] or the magnetic circuit needs to be divided more finely [22][23], which will increase the number of magnetic circuit nodes and make the calculation model more complex. In [1], the equivalent air gap function is used to calculate the AR-MF considering inhomogeneous saturation of the core. However, in many positions where the actual magnetic field is not zero, the analytical calculation result is zero. This is because the equivalent air gap function is in the denominator, which cannot divide zero into non-zero result, leading to inaccurate calculation results.

From the discussion so far, it can be summarized that there are four major problems in computing the AR-MF of IPMSM with segmented skewed poles using existing methods:

- 1) The finite element method is time-consuming.
- 2) The traditional equivalent magnetic circuit method cannot calculate the tangential component of magnetic field.
- 3) The equivalent air gap function method is complex and has a large calculation error.
- 4) The other analytical methods cannot account for saturation effects.

In order to overcome the above limitations, the virtual magnetic field of rotor magnetic barrier is introduced in a novel fashion to calculate the influence of rotor local inhomogeneous saturation on the AR-MF, and the accurate calculation model of AR-MF of IPMSM is established. The accuracy of the calculation model is verified by both finite element simulations and experimentally. The results show that this model can not only ensure the calculation accuracy, but also greatly reduce the computational time.

II. CALCULATION MODEL OF AR-MF OF IPMSM WITH SEGMENTED SKEWED POLES

A. Calculation model of slotless AR-MF without considering saturation

The geometric model of both stator and rotor of the IPMSM with segmented skewed poles considered, is shown in Fig. 1. The stator winding is distributed, and its layout is shown in Fig. 2. The main parameters of the motor are summarized in Table I, and the BH curve of core material is shown in Fig. 3.

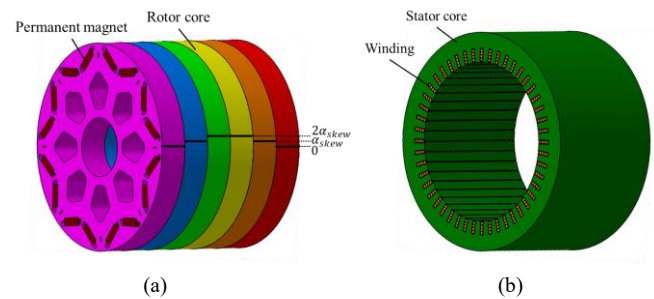


Fig. 1. Geometric model of IPMSM. (a) Rotor with segmented skewed poles. (b) Stator.

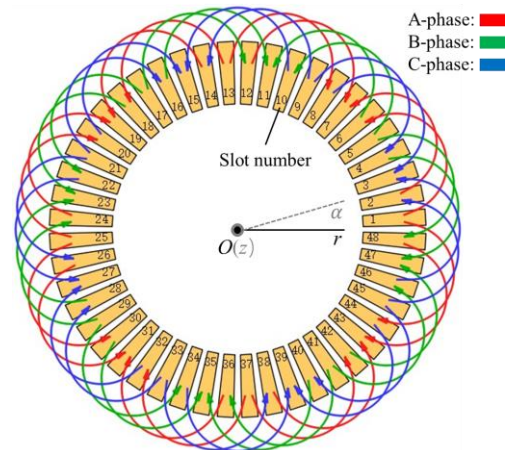


Fig. 2. Stator winding layout.

TABLE I
MOTOR PARAMETERS

Parameter	Symbol	Quantity
Number of pole pairs	p	4
Number of slots	N_s	48
Number of rotor segments	N	6
Skew angle of each segment	α_{skew}	2.5°
Inner radius of stator	R_s	79.8 mm
Outer radius of rotor	R_r	79.1 mm
Slot width	b_{sa}	0.05 rad
Slot opening width	b_{oa}	0.011 rad
Axial length of core	L_z	130 mm
Lamination factor	C_s	0.97
Coil specification	$a \times b$	3.2 mm \times 2.6 mm
Coil layers per slot	N_t	4
Number of parallels	N_p	2
Permeability of vacuum	μ_0	$4\pi \times 10^{-7}$ H/m
Saturation flux density of rotor magnetic barrier	B_s	2 T
Thickness of permanent magnet	h_M	6 mm
Width of permanent magnet	L_M	17 mm
Relative permeability of permanent magnet	μ_r	1.059
Pole arc	α_p	0.558 rad
Width of magnetic barrier	α_b	0.035 rad
Thickness of magnetic barrier at rotor end	h_b	2.1 mm
Thickness of magnetic barrier between poles	h'_b	2.8 mm

> REPLACE THIS LINE WITH YOUR PAPER IDENTIFICATION NUMBER (DOUBLE-CLICK HERE TO EDIT) <

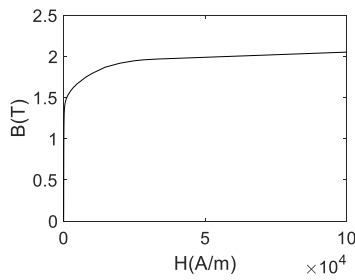


Fig. 3. BH curve of core material.

By using the vector superposition method, the radial and tangential components of the slotless AR-MF without considering saturation can be expressed as:

$$B_{r_us}(z, r, \alpha, t) = \sum_{m=1}^{\infty} B_{mr}(r) \left\{ \sum_{q=A,B,C} \left[I_q(t) \sum_{i=1}^{N_c} S_{qi} \cos m \left(\alpha - \frac{2\pi}{N_s} (\alpha_{qi} - 1) \right) \right] \right\} \quad (1)$$

$$B_{t_us}(z, r, \alpha, t) = \sum_{m=1}^{\infty} B_{mt}(r) \left\{ \sum_{q=A,B,C} \left[I_q(t) \sum_{i=1}^{N_c} S_{qi} \sin m \left(\alpha - \frac{2\pi}{N_s} (\alpha_{qi} - 1) \right) \right] \right\} \quad (2)$$

where, $B_{mr}(r)$ and $B_{mt}(r)$ are the amplitude of m -order radial and tangential flux density at the radial length r , respectively; S_{qi} is the sign vector of magnetomotive force, and α_{qi} is an angle vector, which can be obtained by using the rules in [14]; $I_q(t)$ is the q -phase current at time t ; N_c is the number of coils; z is the axial length; α is the mechanical angle.

B. Calculation model of slotless AR-MF considering saturation

The saturation effect of the rotor magnetic barrier will affect the AR-MF, which is essentially caused by the magnetomotive force drop while the flux lines are crossing the rotor magnetic barrier. The ‘virtual magnetic field of the rotor magnetic barrier’ is introduced to calculate the influence of the saturation effect of the rotor magnetic barrier on the AR-MF.

The subdomain method combined with equivalent magnetic circuit method is used to calculate the virtual magnetic field of rotor magnetic barrier. It is assumed that the stator is not slotted and the permanent magnets do not produce magnetomotive force, and the permeability of the rest of the core is infinite except for the rotor magnetic barriers. The subdomain regions and interface conditions are shown in Fig. 4.

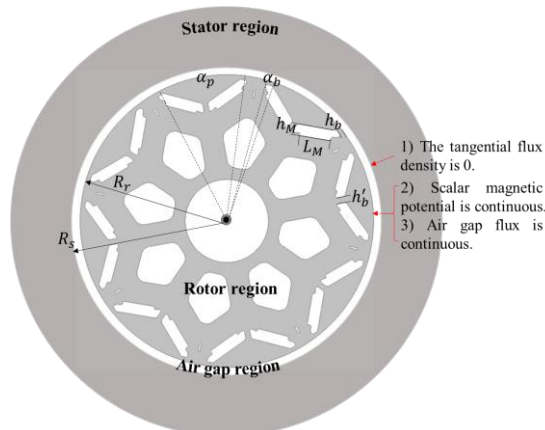


Fig. 4. Subdomain regions and interface conditions.

The radial and tangential components of air gap flux density can be expressed as follows:

$$B_{r_v} = -\sum_{k=1}^{\infty} \frac{k}{r} \left[A_k \left(\frac{r}{R_s} \right)^k + B_k \left(\frac{r}{R_r} \right)^{-k} \right] \sin(k\alpha) + \sum_{k=1}^{\infty} \frac{k}{r} \left[C_k \left(\frac{r}{R_s} \right)^k + D_k \left(\frac{r}{R_r} \right)^{-k} \right] \cos(k\alpha) \quad (3)$$

$$B_{t_v} = -\sum_{k=1}^{\infty} \frac{k}{r} \left[A_k \left(\frac{r}{R_s} \right)^k - B_k \left(\frac{r}{R_r} \right)^{-k} \right] \cos(k\alpha) - \sum_{k=1}^{\infty} \frac{k}{r} \left[C_k \left(\frac{r}{R_s} \right)^k - D_k \left(\frac{r}{R_r} \right)^{-k} \right] \sin(k\alpha) \quad (4)$$

where, A_k , B_k , C_k and D_k are undetermined coefficients.

1) The tangential air gap flux density on the interface between air gap region and stator region is 0.

$$B_{t_v} \Big|_{r=R_s} = 0 \quad (5)$$

By combining (4) and (5), we can get (6):

$$\begin{aligned} A_k - B_k G_k &= 0 \\ C_k - D_k G_k &= 0 \end{aligned} \quad (6)$$

where, $G_k = \left(\frac{R_r}{R_s} \right)^k$.

Writing (5) and (6) in matrix form, we can obtain (7):

$$\begin{aligned} K_{11} A_k + K_{12} B_k &= 0 \\ K_{13} C_k + K_{24} D_k &= 0 \end{aligned} \quad (7)$$

where,

$$\begin{aligned} K_{11} = K_{23} &= \text{diag}(1, 1, \dots, 1)_{K \times K} \\ K_{12} = K_{24} &= \text{diag}(-G_1, -G_2, \dots, -G_k, \dots, -G_K) \end{aligned}$$

2) The scalar magnetic potential at the interface between the air gap region and the rotor region is continuous.

The scalar magnetic potential at the outer radius of the rotor can be expressed as [25]:

$$\begin{aligned} \Omega_r &= \sum_{k=1}^{\infty} \Omega_{rk} \cos[k(\alpha - \alpha_r)] \\ &= \sum_{k=1}^{\infty} \Omega_{rk} \cos(k\alpha_r) \cos(k\alpha) + \sum_{k=1}^{\infty} \Omega_{rk} \sin(k\alpha_r) \sin(k\alpha) \end{aligned} \quad (8)$$

$$\Omega_{rk} = \begin{cases} \Omega_r \Gamma_k(p, \alpha_p, \alpha_b), & k/p \text{ is odd} \\ 0, & k/p \text{ is even} \end{cases} \quad (9)$$

$$\Gamma_k(p, \alpha_p, \alpha_b) = \frac{8p}{k^2 \pi \alpha_b} \sin\left(k \frac{\alpha_p + \alpha_b}{2}\right) \sin\left(k \frac{\alpha_b}{2}\right) \quad (10)$$

> REPLACE THIS LINE WITH YOUR PAPER IDENTIFICATION NUMBER (DOUBLE-CLICK HERE TO EDIT) <

where, α_t is the position of the rotor at time t , and $\alpha_t = \omega t + \alpha_0$; ω is the rotational speed; α_0 is the initial position of the rotor.

The scalar magnetic potential in the air gap region can be obtained by integrating the tangential magnetic field intensity:

$$\Omega_g \Big|_{r=R_r} = \frac{1}{\mu_0} \sum_{k=1}^{\infty} \left[A_k \left(\frac{R_r}{R_s} \right)^k - B_k \right] \sin(k\alpha) - \frac{1}{\mu_0} \sum_{k=1}^{\infty} \left[C_k \left(\frac{R_r}{R_s} \right)^k - D_k \right] \cos(k\alpha) \quad (11)$$

Based on the continuity of scalar magnetic potential at the interface between air gap region and rotor region, we can obtain (12):

$$\begin{cases} \frac{A_k G_k - B_k}{\mu_0} = \Omega_r \Gamma_k(p, \alpha_p, \alpha_b) \sin(k\alpha_t) \\ -\frac{C_k G_k - D_k}{\mu_0} = \Omega_r \Gamma_k(p, \alpha_p, \alpha_b) \cos(k\alpha_t) \end{cases} \quad (12)$$

Writing (12) in matrix form, we can obtain (13):

$$\begin{aligned} K_{31} A_k + K_{32} B_k + K_{35} \Omega_r &= 0 \\ K_{43} C_k + K_{44} D_k + K_{45} \Omega_r &= 0 \end{aligned} \quad (13)$$

where,

$$\begin{aligned} K_{31} &= K_{43} = \text{diag}(G_1, G_2, \dots, G_k, \dots, G_K) \\ K_{32} &= K_{44} = \text{diag}(-1, -1, \dots, -1)_{K \times K} \\ K_{35} &= -\mu_0 [\Gamma_1 \sin(\alpha_t), \Gamma_2 \sin(2\alpha_t), \dots, \Gamma_k \sin(k\alpha_t), \dots, \Gamma_K \sin(K\alpha_t)]^T \\ K_{45} &= \mu_0 [\Gamma_1 \cos(\alpha_t), \Gamma_2 \cos(2\alpha_t), \dots, \Gamma_k \cos(k\alpha_t), \dots, \Gamma_K \cos(K\alpha_t)]^T \end{aligned}$$

3) The air gap flux at the interface between the air gap region and the rotor region is continuous.

The air gap flux on the rotor surface in the air gap region can be expressed as follows:

$$\begin{aligned} \Phi_g &= L_Z \left(A \Big|_{\substack{r=R_r \\ \alpha=\alpha_t+\alpha_w}} - A \Big|_{\substack{r=R_r \\ \alpha=\alpha_t-\alpha_w}} \right) \\ &= \sum_{k=1}^{\infty} (A_k G_{ak} + B_k G_{bk} + C_k G_{ck} + D_k G_{dk}) \sin(k\alpha_w) \end{aligned} \quad (14)$$

where, α_w is the total width of the single magnet and the magnetic barrier, and

$$\begin{aligned} \alpha_w &= \frac{\alpha_p + 2\alpha_b}{2} \\ G_{ak} &= -2L_Z G_k \sin(k\alpha_t) \\ G_{bk} &= -2L_Z \sin(k\alpha_t) \\ G_{ck} &= 2L_Z G_k \cos(k\alpha_t) \\ G_{dk} &= 2L_Z \cos(k\alpha_t). \end{aligned}$$

The equivalent magnetic circuit diagram of rotor region is

shown in Fig. 5.

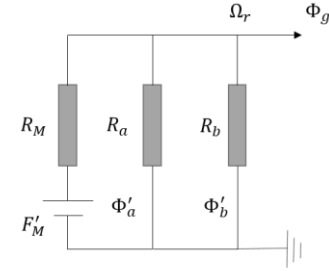


Fig. 5. Equivalent magnetic circuit diagram of rotor region.

The virtual magnetic flux entering the air gap through the rotor surface can be obtained by (15):

$$\Phi_g = -\frac{\Omega_r}{R_M} + \frac{F'_M}{R_M} - \Phi'_a - \Phi'_b \quad (15)$$

where,

F'_M : the virtual permanent magnet magnetomotive force, and $F'_M = 0$;

R_M : the permanent magnet reluctance;

Φ'_a : the virtual leakage flux of magnetic barrier at rotor end;

Φ'_b : the virtual leakage flux of magnetic barrier between poles.

and can be calculated by the following formulas respectively:

$$R_M = \frac{h_M}{\mu_0 \mu_r L_M L_Z} \quad (16)$$

$$\Phi'_a = B'_s h_b L_Z \quad (17)$$

$$\Phi'_b = B'_s \frac{h'_b}{2} L_Z \quad (18)$$

B'_s is the virtual saturation magnetic flux density of magnetic barrier, which can be determined by the following empirical function:

$$B'_s = \begin{cases} 0 & x < 50 \\ 0.03x - 1.5 & x \geq 50 \end{cases} \quad (19)$$

where x is numerically equal to the RMS value of the current in stator winding.

According to the continuity of the air gap flux at the interface between the air gap region and the rotor region, we can be obtained:

$$\sum_{k=1}^{\infty} (A_k G_{ak} + B_k G_{bk} + C_k G_{ck} + D_k G_{dk}) \sin(k\alpha_w) = -\frac{\Omega_r}{R_M} - \Phi'_a - \Phi'_b \quad (20)$$

Writing (20) in matrix form:

$$K_{51} A_k + K_{52} B_k + K_{53} C_k + K_{54} D_k + K_{55} \Omega_r = Y \quad (21)$$

where,

> REPLACE THIS LINE WITH YOUR PAPER IDENTIFICATION NUMBER (DOUBLE-CLICK HERE TO EDIT) <

$$\begin{aligned}
 K_{51} &= [G_{a1} \sin(\alpha_w), G_{a2} \sin(2\alpha_w), \dots, G_{ak} \sin(k\alpha_w), \dots, G_{ak} \sin(K\alpha_w)] \\
 K_{52} &= [G_{b1} \sin(\alpha_w), G_{b2} \sin(2\alpha_w), \dots, G_{bk} \sin(k\alpha_w), \dots, G_{bk} \sin(K\alpha_w)] \\
 K_{53} &= [G_{c1} \sin(\alpha_w), G_{c2} \sin(2\alpha_w), \dots, G_{ck} \sin(k\alpha_w), \dots, G_{ck} \sin(K\alpha_w)] \\
 K_{54} &= [G_{d1} \sin(\alpha_w), G_{d2} \sin(2\alpha_w), \dots, G_{dk} \sin(k\alpha_w), \dots, G_{dk} \sin(K\alpha_w)] \\
 K_{55} &= \frac{1}{R_M} \\
 Y &= -\Phi'_a - \Phi'_b
 \end{aligned}$$

4) By combining (7), (13) and (21), we can obtain (22):

$$\begin{bmatrix} K_{11} & K_{12} & 0 & 0 & 0 \\ 0 & 0 & K_{23} & K_{24} & 0 \\ K_{31} & K_{32} & 0 & 0 & K_{35} \\ 0 & 0 & K_{43} & K_{44} & K_{45} \\ K_{51} & K_{52} & K_{53} & K_{54} & K_{55} \end{bmatrix} \begin{bmatrix} A_k \\ B_k \\ C_k \\ D_k \\ \Omega_r \end{bmatrix} = \begin{bmatrix} 0 \\ 0 \\ 0 \\ 0 \\ Y \end{bmatrix} \quad (22)$$

By solving (22), the undetermined coefficient A_k , B_k , C_k and D_k are obtained. By substituting them into (3) and (4), the radial and tangential components of the virtual magnetic field of the rotor magnetic barrier can be obtained.

The virtual magnetic field of the rotor magnetic barrier is not uniform in the axial direction of the motor due to the segmented skewed poles of the rotor. For the IPMSM with segmented skewed poles, the rotor is divided into N segments in the axial length L , so the length of each segment is $L_z = L/N$. It is assumed that the skewed angle of the j^{th} segment of the rotor with respect to the first segment is β_j , $\beta_j \in \{\beta_1, \beta_2, \dots, \beta_j, \dots, \beta_N\}$. Taking the center of the first end face of the rotor as the origin, a point on any axial length z belongs to the $(\lfloor z/L_z \rfloor + 1)^{\text{th}}$ segment, and its skew angle is $\beta_{\lfloor z/L_z \rfloor + 1}$, where $\lfloor \cdot \rfloor$ denotes rounding down. Then the radial and tangential components of the virtual magnetic field of the IPMSM with segmented skewed poles can be expressed as follows:

$$\begin{aligned}
 B_{r_V}(z, r, \alpha, t) &= - \sum_{k=1}^{\infty} \frac{k}{r} \left[A_k(z, r, \alpha, t) \left(\frac{r}{R_s} \right)^k \right. \\
 &\quad \left. + B_k(z, r, \alpha, t) \left(\frac{r}{R_r} \right)^{-k} \right] \sin[k(\alpha \\
 &\quad + \omega t + \beta_{\lfloor z/L_z \rfloor + 1})] \\
 &\quad + \sum_{k=1}^{\infty} \frac{k}{r} \left[C_k(z, r, \alpha, t) \left(\frac{r}{R_s} \right)^k \right. \\
 &\quad \left. + D_k(z, r, \alpha, t) \left(\frac{r}{R_r} \right)^{-k} \right] \cos[k(\alpha \\
 &\quad + \omega t + \beta_{\lfloor z/L_z \rfloor + 1})] \quad (23)
 \end{aligned}$$

$$\begin{aligned}
 B_{t_V}(z, r, \alpha, t) &= - \sum_{k=1}^{\infty} \frac{k}{r} \left[A_k(z, r, \alpha, t) \left(\frac{r}{R_s} \right)^k \right. \\
 &\quad \left. - B_k(z, r, \alpha, t) \left(\frac{r}{R_r} \right)^{-k} \right] \cos[k(\alpha \\
 &\quad + \omega t + \beta_{\lfloor z/L_z \rfloor + 1})] \\
 &\quad - \sum_{k=1}^{\infty} \frac{k}{r} \left[C_k(z, r, \alpha, t) \left(\frac{r}{R_s} \right)^k \right. \\
 &\quad \left. - D_k(z, r, \alpha, t) \left(\frac{r}{R_r} \right)^{-k} \right] \sin[k(\alpha \\
 &\quad + \omega t + \beta_{\lfloor z/L_z \rfloor + 1})] \quad (24)
 \end{aligned}$$

By adding the slotless AR-MF without considering saturation and the virtual magnetic field of the rotor magnetic barrier, the slotless AR-MF considering saturation can be obtained:

$$B_{r_{-AR}}(z, r, \alpha, t) = B_{r_{-us}}(z, r, \alpha, t) + B_{r_V}(z, r, \alpha, t) \quad (25)$$

$$B_{t_{-AR}}(z, r, \alpha, t) = B_{t_{-us}}(z, r, \alpha, t) + B_{t_V}(z, r, \alpha, t) \quad (26)$$

C. Calculation model of slotted AR-MF considering saturation

By introducing the 3-D complex relative permeance to calculate the stator slotting effect [24], the radial and tangential components of slotted AR-MF of IPMSM with segmented skewed poles can be obtained:

$$B_{ar}(z, r, \alpha, t) = B_{r_{-AR}}(z, r, \alpha, t) \lambda_a(z, r, \alpha) + B_{t_{-AR}}(z, r, \alpha, t) \lambda_b(z, r, \alpha) \quad (27)$$

$$B_{at}(z, r, \alpha, t) = B_{t_{-AR}}(z, r, \alpha, t) \lambda_a(z, r, \alpha) - B_{r_{-AR}}(z, r, \alpha, t) \lambda_b(z, r, \alpha) \quad (28)$$

where, λ_a is the real part of complex relative permeance, λ_b is the imaginary part of complex relative permeance.

III. FE VERIFICATION AND CHARACTERISTIC ANALYSIS OF AR-MF

The armature reaction electromagnetic finite element model of an 8-pole 48-slot IPMSM with segmented skewed poles for electric vehicle is established. The sinusoidal current excitation with RMS value of 150 A and lead angle of 46° is applied in the stator winding. The rotor initial angle is 3.75° . The calculation cycle is a mechanical cycle at rated speed condition and the number of calculation steps is 960. It takes 35 minutes for calculation with the proposed model and 420 minutes for finite element simulation under the same calculation conditions.

The spatial distribution and order of AR-MF of IPMSM are shown in Fig. 6. Compared with the results of finite element method, the accuracy of calculation model without considering saturation (M1) is 81.78%, and the accuracy of calculation model considering saturation (M2) is 99.49% (calculated by coefficient of determination). The spatial orders of AR-MF mainly include 4, 12, 20, 28, 36 and so on, satisfying $k = (2n - 1)p$, where n is a positive integer and p is the number of pole pairs.

> REPLACE THIS LINE WITH YOUR PAPER IDENTIFICATION NUMBER (DOUBLE-CLICK HERE TO EDIT) <

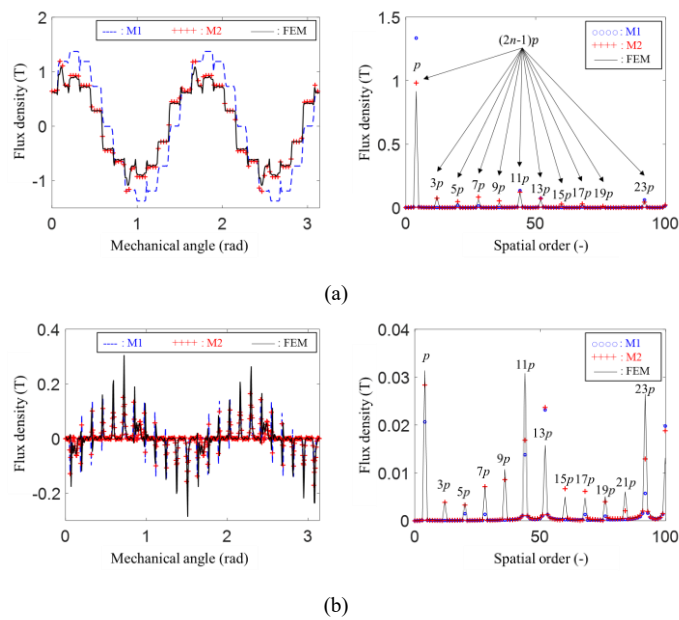


Fig. 6. Spatial distribution and order of AR-MF. (a) Radial component. (b) Tangential component.

The temporal variation and amplitude-frequency characteristics of AR-MF of IPMSM are shown in Fig. 7. Compared with the results of finite element method, the accuracy of calculation model without considering saturation (M1) is 67.67%, and the accuracy of calculation model considering saturation (M2) is 99.74%. The frequencies of AR-MF are mainly 340 Hz, 1020 Hz, 1700 Hz, 2380 Hz, 3060 Hz and so on, satisfying $f = (2n - 1)f_0$, where n is a positive integer and f_0 is the fundamental frequency.

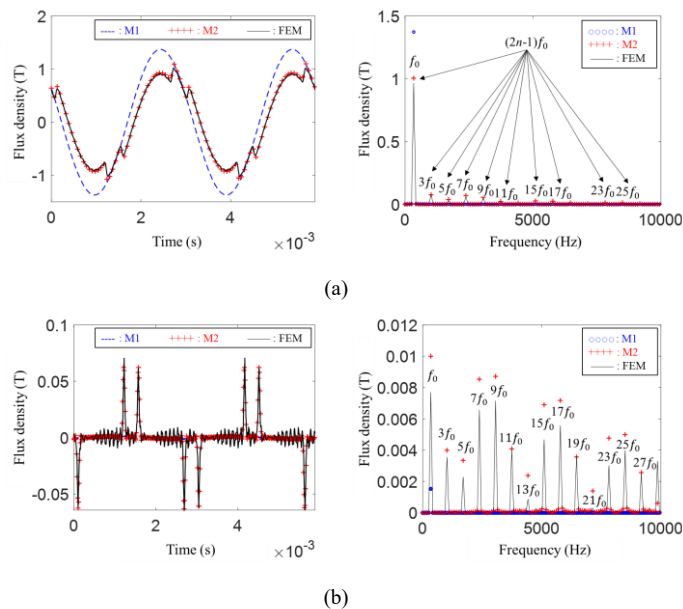


Fig. 7. Time variation and amplitude-frequency characteristics of AR-MF. (a) Radial component. (b) Tangential component.

According to the 3-D spatial distribution of AR-MF of IPMSM with segmented skewed poles shown in Fig. 8, the change of AR-MF along the axial length of the motor is uneven. Although the stator is not segmented, the virtual magnetic field

of the rotor magnetic barrier generated by the rotor changes along the axial length of the motor. The virtual magnetic field of the rotor magnetic barrier has an impact on the AR-MF, resulting in the phenomenon of stratification of the AR-MF. The rotor has 6 segments, and the skewed angle of each segment is 2.5° . Therefore, in the axial direction of the motor, the results show that the AR-MF also shows 6-segment stratification, and the adjacent segments are staggered by 2.5° in space.

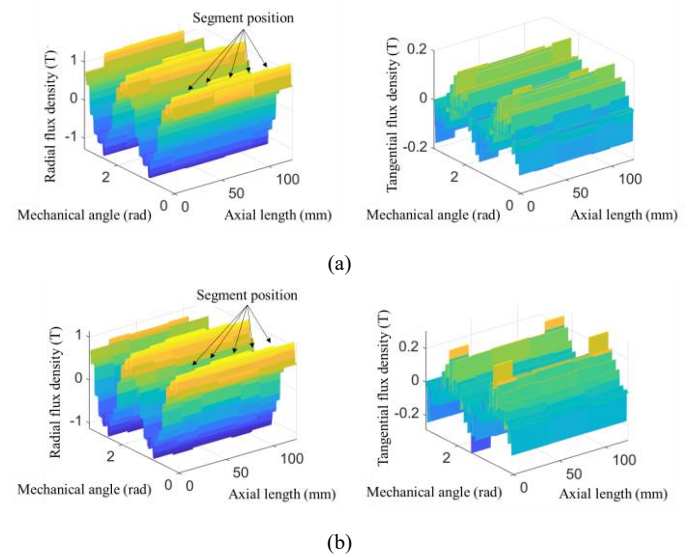


Fig. 8. The 3-D spatial distribution of AR-MF. (a) Calculation results. (b) Finite element simulation results.

IV. VERIFICATION OF INDUCTANCE AND ELECTROMAGNETIC TORQUE

A. Verification of inductance

Based on the armature reaction magnetic field, the self-inductance and mutual inductance of each phase winding can be calculated by [14]:

$$L_{XX} = \frac{LR_s}{2I_X} \int_0^{2\pi} N_X B_{ar_X} d\alpha \quad (29)$$

$$L_{XY} = \frac{LR_s}{2I_Y} \int_0^{2\pi} N_X B_{ar_Y} d\alpha \quad (30)$$

where, I_X and I_Y represent currents of the X-phase and Y-phase windings respectively; N_X represents windings function of the X-phase; B_{ar_X} and B_{ar_Y} represent the radial component of armature reaction magnetic field generated by X-phase and Y-phase windings respectively.

In order to verify the accuracy of the calculation model, the self and mutual inductance of each phase winding under sinusoidal current excitation with different RMS values are calculated. Since the self-inductance of each phase winding has the same amplitude and change trend, the self-inductance L_{AA} is selected as an example. Similarly, the mutual inductance L_{AB} is selected. The calculation results are shown in Fig. 9. The calculation results are in good agreement with the finite element

> REPLACE THIS LINE WITH YOUR PAPER IDENTIFICATION NUMBER (DOUBLE-CLICK HERE TO EDIT) <

simulation results. Compared with the finite element simulation results, the error of the calculation results is less than 8%.

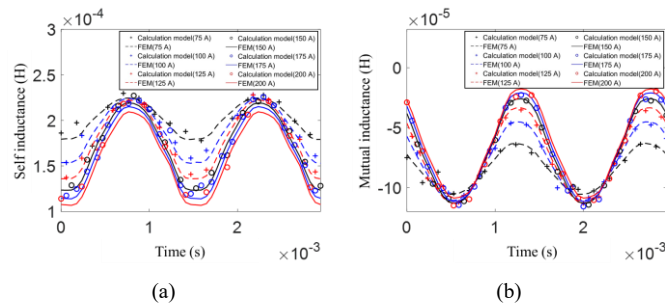


Fig. 9. Self and mutual inductance. (a) Self-inductance (L_{AA}). (b) Mutual inductance (L_{AB}).

B. Verification of electromagnetic torque

The electromagnetic torque of IPMSM with segmented skewed poles can be calculated by the following expression:

$$T_{em} = \frac{Lr^2}{\mu_0} \int_0^{2\pi} (B_{mr} + B_{ar})(B_{mt} + B_{at}) d\alpha \quad (31)$$

where B_{mr} and B_{mt} are the radial and tangential components of the open circuit air gap magnetic field, respectively, and can be obtained by the method proposed in [24].

The accuracy of calculation results of AR-MF of IPMSM with segmented skewed poles can be indirectly verified by electromagnetic torque measurement. The photo of the experimented motor is shown in Fig. 10. The electromagnetic torque measurement system is shown in Fig. 11. The IPMSM under test is used as prime mover and servo motor as load. The speed and torque of the tested IPMSM are controlled to achieve the test target condition, and the torque is recorded in real time. The experimental setup is shown in Fig. 12.

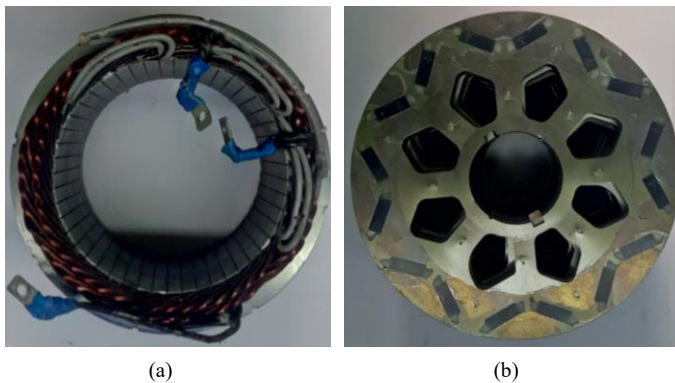


Fig. 10. The experimented motor. (a) Stator. (b) Rotor.

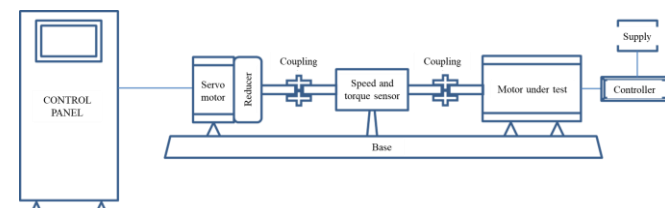


Fig. 11. The electromagnetic torque measurement system.

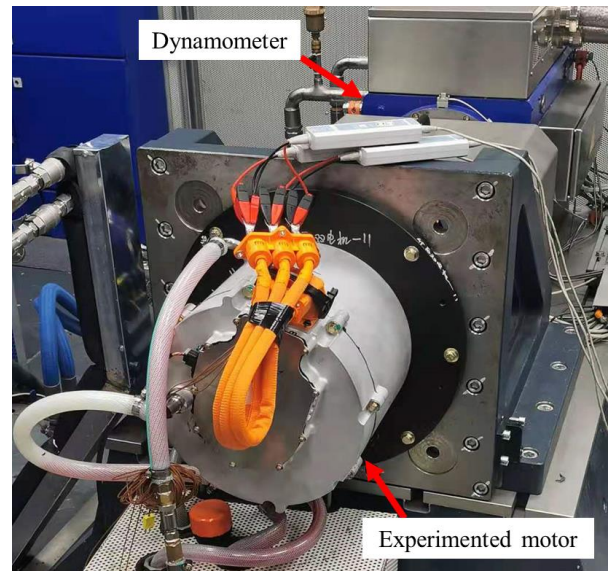


Fig. 12. The experimental setup.

The calculation model, finite element simulation and measurement results of electromagnetic torque under the operating conditions of sinusoidal winding current with RMS value of 0-200 A at constant speed of 5100 rpm are shown in Fig. 13. The results of calculation model and finite element simulation are in good agreement with the experimental results, and the latter is slightly smaller, which is due to the influence of mechanical friction torque of motor. Compared with the experimental results, the error of calculation results is 2.11%, and that of finite element simulation is 0.39%. The results of electromagnetic torque measurement indirectly verify the accuracy of the calculation model of AR-MF.

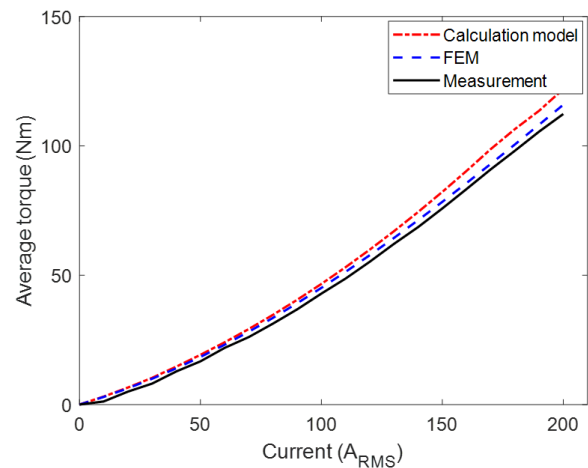


Fig. 13. Average torque vs current characteristic comparison: calculation model, finite element simulation (FEM) and measurement results.

V. CONCLUSION

In this paper, the influence of local inhomogeneous saturation effect of rotor magnetic barrier on AR-MF is quantitatively calculated by using the virtual magnetic field calculation model of rotor magnetic barrier. At the same time, the influence of stator slotting effect on AR-MF is

> REPLACE THIS LINE WITH YOUR PAPER IDENTIFICATION NUMBER (DOUBLE-CLICK HERE TO EDIT) <

quantitatively calculated by introducing complex relative permeance. An accurate calculation model of AR-MF of IPMSM with segmented skewed poles is therefore established, and the main conclusions are as follows:

- 1) This calculation model can take the saturation effect of rotor magnetic barrier and the slotting effect of stator into consideration. Moreover, it can calculate the 3-D spatial distribution of AR-MF of IPMSM with segmented skewed poles along the axial and circumferential direction of the motor.
- 2) The main spatial order of the AR-MF satisfies $k = (2n - 1)p$, where n is a positive integer and p is the number of pole pairs; the main frequency of the AR-MF satisfies $f = (2n - 1)f_0$, where f_0 is the fundamental frequency. The AR-MF of the IPMSM with segmented skewed poles presents N -segment stratification in the axial direction of the motor, and N is the number of rotor segments; the AR-MF of adjacent segments are staggered by an angle of α_{skew} in space, and α_{skew} is the skew angle.
- 3) Compared with the finite element method, the accuracy of the calculation model is more than 99% in alignment, while the time consumption is less than 10% of the finite element method. This model can greatly shorten the calculation time while ensuring the calculation accuracy.

REFERENCES

- [1] M. Farshadnia, and M. Cheema, R. Dutta, and J. Fletcher. "Analytical Modeling of Armature Reaction Air-Gap Flux Density Considering the Non-Homogeneously Saturated Rotor in a Fractional-Slot Concentrated-Wound IPM Machine," *IEEE Trans. Magn.*, vol. 53, no. 2, pp. 8200412, Feb. 2017.
- [2] F. Ma, H. Yin, L. Wei, L. Wu, and C. Gu, "Analytical Calculation of Armature Reaction Field of the Interior Permanent Magnet Motor," *energies*, vol. 11, no. 2375, pp. 1-12, Sep. 2018.
- [3] S. Zhu, W. Chen, M. Xie, C. Liu, and K. Wang, "Electromagnetic Performance Comparison of Multi-Layered Interior Permanent Magnet Machines for EV Traction Applications," *IEEE Trans. Magn.*, vol. 54, no. 11, pp. 8104805, Nov. 2018.
- [4] B. Guo, Y. Huang, F. Peng, and J. Dong, "A New Hybrid Method for Magnetic Field Calculation in IPMSM Accounting for Any Rotor Configuration," *IEEE Trans. Ind. Electron.*, vol. 66, no. 7, pp. 5015-5024, Jul. 2019.
- [5] S. Wu, L. Guo, H. Wang, Y. Cao, T. Shi, and C. Xia, "Inductance Calculation of Interior Permanent Magnet Machines Considering Asymmetrical Saturation of the Bridge," *IEEE Trans. Magn.*, vol. 55, no. 11, pp. 8107511, Nov. 2019.
- [6] K. Yamazaki, R. Suzuki, M. Nuka, and M. Masegi, "Analysis and Characteristics Improvement of Claw-Pole Alternators by Reducing Armature Reaction," *IEEE Trans. Ind. Electron.*, vol. 65, no. 11, pp. 8740-8748, Nov. 2018.
- [7] Y. Zheng, L. Wu, H. Li, H. Wen, and L. Qiu, "Harmonic Analysis of Airgap Magnetic Fields in Doubly-Fed Flux Reversal Permanent Magnet Machines," *IEEE Access*, vol. 8, no. 1, pp. 134856-134867, Jul. 2020.
- [8] P. Su, W. Hua, Z. Wu, P. Han, and M. Cheng, "Analysis of the Operation Principle for Rotor-Permanent-Magnet Flux-Switching Machines," *IEEE Trans. Ind. Electron.*, vol. 65, no. 2, pp. 1062-1073, Feb. 2018.
- [9] J. Zheng, W. Zhao, J. Ji, J. Zhu, C. Gu, and S. Zhu, "Design to Reduce Rotor Losses in Fault-Tolerant Permanent-Magnet Machines," *IEEE Trans. Ind. Electron.*, vol. 65, no. 11, pp. 8476-8487, Nov. 2018.
- [10] X. Zhu, W. Hua, B. Wang, and N. Dai, "Comparison of stator- and rotor-surface-mounted PM brushless machines," *IET Electr. Power Appl.*, vol. 14, no. 1, pp. 62-70, Nov. 2019.
- [11] M. Cheng, X. Zhu, Y. Wang, R. Wang, and W. Wang, "Effect and Inhibition Method of Armature-Reaction Field on Superconducting Coil in Field-Modulation Superconducting Electrical Machine," *IEEE Trans. Energy Convers.*, vol. 35, no. 1, pp. 279-291, Mar. 2020.

- [12] P. Su, W. Hua, M. Hu, Z. Chen, M. Cheng, and W. Wang, "Analysis of PM Eddy Current Loss in Rotor-PM and Stator-PM Flux-switching Machines by Air-gap Field Modulation Theory," *IEEE Trans. Ind. Electron.*, vol. 67, no. 3, pp. 1824-1835, Mar. 2020.
- [13] Y. Wang, W. Xu, X. Zhang, and W. Ma, "Harmonic Analysis of Air Gap Magnetic Field in Flux-Modulation Double-Stator Electrical-Excitation Synchronous Machine," *IEEE Trans. Ind. Electron.*, vol. 67, no. 7, pp. 5302-5312, Jul. 2020.
- [14] C. Ma, Q. Li, H. Lu, Y. Liu, and H. Gao, "Analytical model for armature reaction of outer rotor brushless permanent magnet DC motor," *IET Electr. Power Appl.*, vol. 12, no. 5, pp. 651-657, Mar. 2018.
- [15] W. Deng, and S. Zuo, "Comparative Study of Sideband Electromagnetic Force in Internal and External Rotor PMSMs With SVPWM Technique," *IEEE Trans. Ind. Electron.*, vol. 66, no. 2, pp. 956-966, Feb. 2019.
- [16] M. Pourahmadi-Nakhli, A. Rahideh, and M. Mardaneh, "Analytical 2-D Model of Slotted Brushless Machines With Cubic Spoke-Type Permanent Magnets," *IEEE Trans. Energy Convers.*, vol. 33, no. 1, pp. 373-382, Mar. 2018.
- [17] Z. Djelloul-Khedda, K. Boughrara, F. Dubas, A. Kechroud, and B. Souleyman, "Semi-Analytical Magnetic Field Predicting in Many Structures of Permanent-Magnet Synchronous Machines Considering the Iron Permeability," *IEEE Trans. Magn.*, vol. 54, no. 7, pp. 8103921, Jul. 2018.
- [18] A. Vahaj, A. Rahideh, H. Moayed-Jahromi, and A. Ghaffari, "Exact Two-Dimensional Analytical Calculations for Magnetic Field, Electromagnetic Torque, UMF, Back-EMF, and Inductance of Outer Rotor Surface Inset Permanent Magnet Machines," *Math. Comput. Appl.*, vol. 24, no. 24, pp. 1-25, Feb. 2019.
- [19] H. Zhang, Z. Deng, M. Yang, Y. Zhang, J. Tuo, and J. Xu, "Analytical Prediction of Halbach Array Permanent Magnet Machines Considering Finite Tooth Permeability," *IEEE Trans. Magn.*, vol. 56, no. 6, pp. 8101010, Jun. 2020.
- [20] S. Min, G. Bramerdorfer, and B. Sarlioglu, "Analytical Modeling and Optimization for Electromagnetic Performances of Fractional-Slot PM Brushless Machines," *IEEE Trans. Ind. Electron.*, vol. 65, no. 5, pp. 4017-4027, May. 2018.
- [21] S. Lee, S. Kim, P. Han, and C. Kim, "Equivalent Circuit Analysis of Induction Motors Considering Magnetic Saturation for Automotive Applications," *J. Electr. Eng. Technol.*, vol. 15, no. 1, pp. 1663-1668, Apr. 2020.
- [22] H. Saneie, and Z. Nasiri-Gheidari, "Performance Analysis of Outer-Rotor Single-Phase Induction Motor Based on Magnetic Equivalent Circuit," *IEEE Trans. Ind. Electron.*, vol. 68, no. 2, pp. 1046-1054, Feb. 2021.
- [23] P. Naderi, and A. Shiri, "Modeling of Ladder-Secondary-Linear Induction Machine Using Magnetic Equivalent Circuit," *IEEE Trans. Veh. Technol.*, vol. 67, no. 12, pp. 11411-11419, Dec. 2018.
- [24] C. Ma, Y. An, H. Zhao, S. Guo, X. Yin, and H. Lu, "3-D Analytical Model and Direct Measurement Method of Ultra-thin Open-circuit Air-gap Field of Interior Permanent Magnet Synchronous Motor with Multi-segmented Skew Poles and Multi-layered Flat Wire Windings for Electric Vehicle," *IEEE Trans. Energy Convers.*, vol. 35, no. 3, pp. 1316-1326, Sep. 2020.
- [25] Z. Zhang, C. Xia, Y. Yan, Q. Geng, and T. Shi, "A Hybrid Analytical Model for Open-circuit Field Calculation of Multilayer Interior Permanent Magnet Machines," *J. Magn. Magn. Mater.*, vol. 435, no. 1, pp. 136-145, Mar. 2017.



Yuansheng An was born in Shandong, China, in 1991. He received the B.E. and M.E. degrees in automotive engineering from Shandong University of Science and Technology in 2014, and from Harbin Institute of Technology-Weihai in 2020, respectively. He is currently working toward the Ph.D. degree in School of Automotive Engineering, Harbin Institute of Technology-Weihai, Weihai, China.

His research interests include vehicle vibration and noise control, and vibration and noise of electrical machines.

> REPLACE THIS LINE WITH YOUR PAPER IDENTIFICATION NUMBER (DOUBLE-CLICK HERE TO EDIT) <



Conggan Ma (M'14) was born in Sichuan, China, in 1987. He received the B.S.E. and Ph.D. degrees in automotive engineering from Tongji University, Shanghai, China, in 2010 and 2014, respectively.

Since 2019, he has been a professor with the Automotive Engineering College, Harbin Institute of Technology-Weihai, Weihai, China, where he was an associate professor from 2014 to 2019. His research interests include vehicle system dynamics and control, vehicle vibration and noise control, and vibration and noise of electrical machines.

Professor Ma is a senior member of IEEE, a member of IEEE Vehicular Technology Society, a member of the Chinese Society of Theoretical and Applied Mechanics, and a member of the Society of Automotive Engineering of China. He is a senior member of the Chinese Society for Vibration and Engineering.



Nic Zhang is lecturer in Data Science and Artificial Intelligence at University of Bath, United Kingdom. He received his BEng degree in Vehicle Engineering from Tongji University of Shanghai, China in 2010, and his MSc in Automotive Engineering in 2011 and PhD in Mechanical Engineering in 2016 from University of Bath, UK.

He has a wide research interests in automotive powertrain systems and automated driving systems. He has a wide range of industry experience through employment with Schaeffler Group, FEV GmbH and Jaguar Land Rover and various engineering consultancy projects for Ford Motors, Cummins, Honeywell, BorgWarner, etc.



Yue Guo (M'10) was born in Beijing, China, in 1983. He received the BEng degree in Electrical Engineering and Automation from Harbin Institute of Technology, Harbin, China, in 2004. After his undergraduate degree, he studied in the School of Computer Science at the University of Nottingham where he received an MSc in Management of Information Technology in 2005. He then successfully completed a PhD in Model Based design for Automotive Electronic System at the University of Warwick in 2009. He also received an MBA degree from Warwick Business School (WBS) in 2018.

He has worked closely and extensively with the automotive industry on multiple collaborative research projects focusing on System of Systems modelling, automated model based testing, battery modelling and characterization by using new and existing techniques. His research interests include system modelling, robust design and validation of automotive electronic system, advanced testing techniques applied to Li-ion batteries and the design of energy storage systems for low carbon vehicles. In 2019, he is appointed as Chair Professor of Battery Systems at the Centre for Advanced Low Carbon Propulsion Systems (C-ALPS) in the Institute of Future Transport and Cities at Coventry University.

Professor Guo is a Chartered Engineer, Senior Member of IEEE, Member of IET, and Committee Member of SAE International Battery Thermal Management Committee.



Michele Degano (M'10) was born in Italy, in 1983. He received the Laurea degree in electrical engineering from the University of Trieste, Trieste, Italy, in 2011, and the Ph.D. degree in industrial engineering from the University of Padova, Padova, Italy, in 2015.

In 2015, he joined the Power Electronics, Machines and Control Group, The University of Nottingham, Nottingham, U.K., as a Research Fellow. Since 2016, he has been an Assistant Professor with the Department of Electrical and Electronic Engineering at the University of Nottingham. His research interests include design and optimization of permanent-magnet machines, reluctance and permanent-magnet-assisted synchronous reluctance motors through genetic optimization techniques, for industrial, automotive and aerospace applications, ranging from small to large power.



Chris Gerada (M'05) was born in Malta, in 1978. He received the Ph.D. degree in numerical modeling of electrical machines from The University of Nottingham, Nottingham, U.K., in 2005.

He subsequently was a Researcher with The University of Nottingham on high-performance electrical drives and on the design and modeling of electromagnetic actuators for aerospace applications. Since 2006, he has been the Project Manager of the GE Aviation Strategic Partnership. In 2008, he was appointed as a Lecturer in electrical machines; in 2011, as an Associate Professor; and in 2013, as a Professor at The University of Nottingham. His main research interests include the design and modeling of high-performance electric drives and machines.

Dr. Gerada serves as an Associate Editor for the IEEE Transactions on Industry Applications and is the Chair of the IEEE IES Electrical Machines Committee.



Feifei Bu (M'11) was born in Maanshan, China, in 1984. He received the B.S. degree in electrical engineering from Anhui University of Technology, Maanshan, China, in 2006, and the Ph.D. degree (master-doctorate program) in electrical engineering from Nanjing University of Aeronautics and Astronautics, Nanjing, China, in 2014.

He joined the faculty of the Department of Electrical Engineering, NUAU, in 2014, where he is currently an Associate Professor. His research interests include power electronics and electrical machines for standalone power systems, renewable energy generating systems, electric vehicle driving systems, etc.

> REPLACE THIS LINE WITH YOUR PAPER IDENTIFICATION NUMBER (DOUBLE-CLICK HERE TO EDIT) <



Xiangrui Yin was born in Heilongjiang, China, in 1992. He received the B.Sc. and M.Sc. degrees in Electrical Engineering & Automation from Harbin Institute of Technology, Harbin, China, in 2014 and 2017, respectively.

Since 2017, he has been an Engineer with the Electric Drive System Institute of FAW, China. His research interests include electromagnetic design of EV motors and performance development of EV drive system.



Qiongyao Li was born in Shaanxi, China, in 1994. She received the B.S.E. and M.E. degrees in automotive engineering from Harbin Institute of Technology, Weihai, China, in 2016 and in 2019, respectively. She is currently working toward the Ph.D. degree in School of Automotive Engineering, Harbin Institute of Technology-Weihai, Weihai, China.

Her research interests include vehicle vibration and noise control, and vibration and noise of electrical machines.



Shengsen Zhou was born in Shandong, China, in 1995. He received the B.S.E. degree and M.E. degrees in automotive engineering from Harbin Institute of Technology, Weihai, China, in 2018 and in 2020, respectively. He is currently working toward the Ph.D. degree in School of Automotive Engineering, Harbin Institute of Technology-Weihai, Weihai, China.

His research interests include vehicle vibration and noise control, and vibration and noise of electrical machines.